Molecular Therapy
Nucleic Acids
Original Article

Exploring the therapeutic potential of sγPNA-141: Pharmacodynamics and mechanistic insights during ischemic stroke recovery

Sanjeev Kumar Yadav,[1] Karishma Dhuri,[2] Daylin Gamiotea-Turro,[1] Mary-Katherine Cormier,[1] Vraj Patel,[1] Arun Kumar Yadawa,[1] Mounika Pathuri,[2] Raman Bahal,[2] and Rajkumar Verma[1]

[1]Department of Neuroscience, UConn Health, Farmington, CT 06032, USA; [2]School of Pharmacy, University of Connecticut, Storrs, CT 06269, USA

MicroRNA-141-3p plays a detrimental role in the pathology of ischemic stroke, presenting a new target for stroke treatment. This study introduces and validates a novel class of peptide nucleic acid (PNA)-based miR-141-3p inhibitors known as serine gamma PNA-141 (sγPNA-141) for ischemic stroke treatment. After synthesis, physicochemical characterization, and nanoparticle encapsulation of sγPNA-141, we compared its safety and efficacy with traditional phosphorothioate- and regular PNA-based anti-miR-141-3p (PNA-141) *in vitro*, followed by detailed *in vivo* and *ex vivo* efficacy testing of sγPNA-141 for treating ischemic stroke using a mouse model. sγPNA-141 demonstrated higher affinity and specificity toward miR-141-3p, and when applied post-stroke, demonstrated decreased brain damage, enhanced neuroprotective proteins, reduced tissue atrophy, swift improvement in functional deficits, and improvement in learning and memory during long-term recovery. Overall, our data show sγPNA-141 has neuroprotective and neuro-rehabilitative effects during stroke recovery. Furthermore, we demonstrated sγPNA-141's effects are mediated by the TGF-β-SMAD2/3 pathway. In summary, the present findings suggest that sγPNA-141 could be a potentially novel and effective therapeutic modality for the treatment of ischemic stroke.

INTRODUCTION

Ischemic stroke is the leading cause of long-term disability around the world and is characterized by the sudden onset of neurological deficits following stroke.[1] Disability resulting from stroke poses a significant economic burden on both the victims and their family members. Despite recent advancements, there is a notable absence of therapeutic drug interventions to mitigate brain damage and facilitate post-stroke recovery. The existing therapeutic gap underscores the pressing need to identify and validate new targets and synthesize novel experimental drugs aimed at enhancing stroke recovery.

Small RNAs such as microRNAs (also known as miRNAs or miRs) have been identified as promising therapeutic targets due to their potential regulatory roles in multiple diseases, including stroke.[2,3] Single-stranded mature miRs bind to the 3′ untranslated region (UTR) of mRNAs through complementary sequences, inducing either mRNA decay or translation inhibition.[4,5] A single miR often regulates multiple downstream target mRNA, and its function is highly conserved across species. Together, these unique features render miRs a potential therapeutic target for neurological disorders, including ischemic stroke.[6]

In 2008, Jeyaseelan et al. conducted the first miR profiling study in cerebral ischemia, catalyzing promising research on miRs in the context of ischemic stroke.[7] Following ischemic stroke, several profiling studies showed dysregulation of various miRs, including miR-124, miR-424, miR-let-7c-5p, miR-155, miR-181c, and miR-132, in different tissues and body fluids.[8] A few studies have attempted to demonstrate the *in vivo* efficacy of modulating these miRs to mitigate post-stroke injury, but these remain limited to acute outcomes.[9,10] To date, few studies have studied the impact of commercially available synthetic miR inhibitors or miR-based sponges on neuroprotection and long-term behavioral recovery following stroke.[10,11]

In prior studies, we found that miR-141-3p expression was significantly upregulated in mice brain tissue for up to 2 weeks after an ischemic stroke.[12] Our work revealed that blocking miR-141-3p with systemic administration of the commercially available inhibitor for miR-141-3p reduced stroke-induced acute infarct injury.[12,13] Furthermore, anti-miR-141 treatment also rescued from the detrimental effect of post-stroke social isolation in aged animals, the population most at risk for stroke and post-stroke isolation.[12] Despite these promising results and the availability of various miR-141-3p inhibitors, the therapeutic interventions of miR inhibitors face several limitations. These include the need for viral or non-viral transfection reagents for cell penetration, *in vivo* instability, and toxicity.[14] In a nutshell, these challenges highlight the need for the development of a different class of miR inhibitors that overcome the aforementioned limitations.

Received 3 May 2024; accepted 2 October 2024;
https://doi.org/10.1016/j.omtn.2024.102355.

Correspondence: Raman Bahal, School of Pharmacy, University of Connecticut, Storrs, CT 06269, USA.
E-mail: raman.bahal@uconn.edu
Correspondence: Rajkumar Verma, Department of Neuroscience, UConn Health, Farmington, CT 06032, USA.
E-mail: raverma@uchc.edu

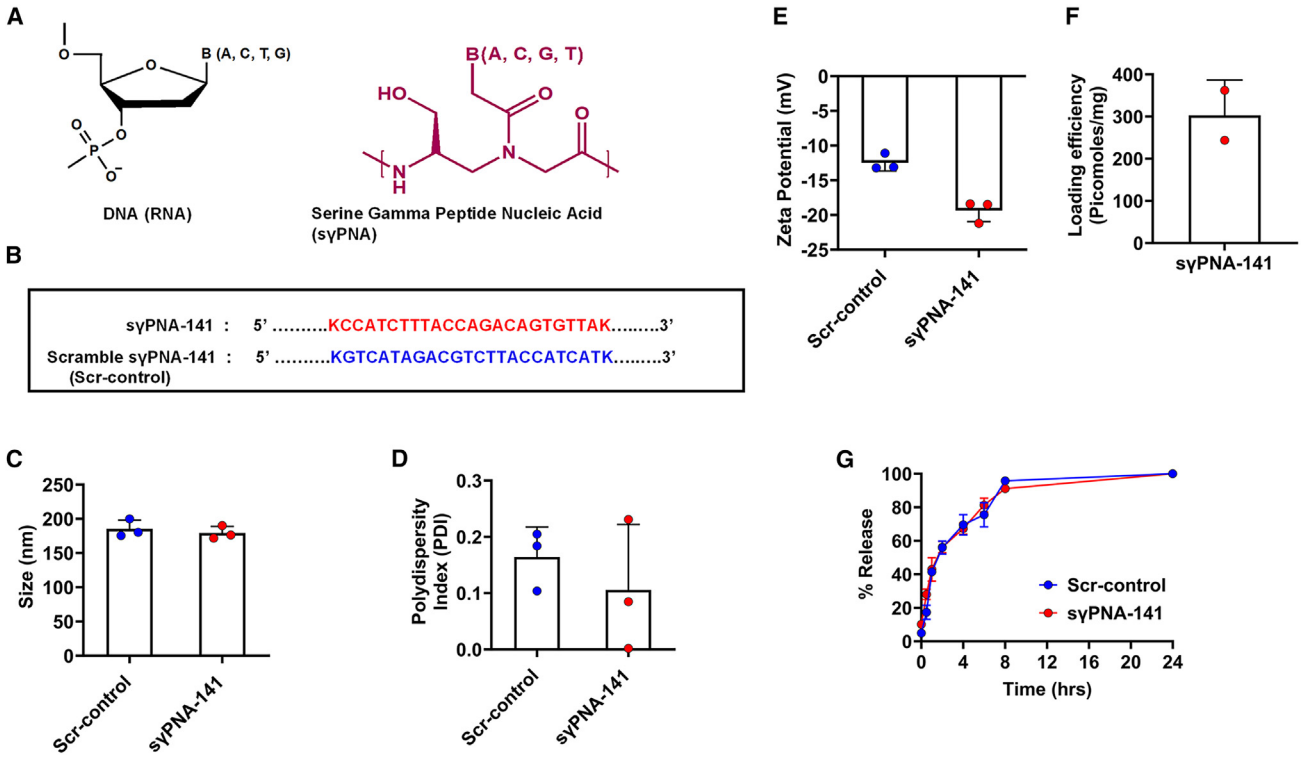

Figure 1. Synthesis and characterization of serine gamma PNA-based NPs containing anti-miR-141-3p sequences

Chemical structure of sγPNA and the oligomer sequence of sγPNA-141 and scramble sγPNA-141 (scr-control) (A and B). Mean hydrodynamic diameter and polydispersity index (PDI) were measured using dynamic light scattering (DLS), and the surface charge was assessed using zeta potential (C–E). sγPNA-141 loading analysis and cumulative release profile data of sγPNA-141 and scr-sγPNA (F and G). All experiments performed in triplicates. Data are shown as mean ± standard deviation (SD).

Among the different classes of anti-miR moieties, phosphorothioate (PS) is a well-known first-generation modified antisense oligonucleotide (ASO) in which a sulfur atom replaces non-bridging oxygen.[15] PS molecules can degrade the target RNA by RNase H cleavage activity.[16] Similarly, peptide nucleic acids (PNAs) are another family of ASOs in which modification occurs in the PNA backbone.[17] In regular PNAs, the sugar-phosphate backbone is swapped by a peptide that provides nuclease resistance and high binding affinity due to a neutral charge.[18] PNAs block the interaction of target mRNA with the ribosome by steric hindrance.[19] PNAs have been widely utilized to specifically target a variety of miRNAs that are overexpressed in cardiovascular diseases and cancers.[20,21] In this study, we use serine gamma PNAs (sγPNAs), which are advanced and modified PNAs in which a chiral center at the gamma position of the PNA backbone is installed. This modification preorganizes the PNA into a right-handed helical conformation, which further enhances its binding affinity to complementary target sites via Watson-Crick base pairing. sγPNA contains a hydroxy group as a side chain at the gamma position of the backbone, further enhancing their solubility and binding affinity compared with regular PNA.[22] In a comparative study of the efficacy of short anti-seed regular PNA, diethylene glycol gamma PNA and sγPNA conjugated to pH-low insertion peptide have been tested after systemic delivery.[23] The serine gamma-modified PNAs exhibited greater thermal melting temperature than regular PNA, suggesting that sγPNA-based anti-miRs have enhanced binding affinity (Figure 1; Table S1). Hence, here, we synthesized, developed, and optimized a next-generation, chemically modified PNA-based anti-miR-141-3p called serine gamma PNA-141 (sγPNA-141) for stroke therapy. We encapsulated sγPNA-141 in poly(lactide-co-glycolide) (PLGA)-based nanoparticles (NPs) to facilitate cellular uptake. We hypothesized that due to the high affinity of sγPNA-based inhibitors for miR-141-3p, these inhibitors will be more potent and effective neuroprotective agents. To test our hypothesis, we delivered the NPs containing sγPNA-141 inhibitor in the mice after ischemic stroke induced by the middle cerebral artery occlusion (MCAo) method. We also assessed acute and long-term recovery and tested downstream targets of miR-141-3p to unravel its mechanism of action. To our knowledge, this is the first report to evaluate NPs containing sγPNA-based miR-141-3p inhibitors for treatment of ischemic stroke and the first to evaluate both acute and long-term impacts of any miR-141-3p inhibitors.

RESULTS

Design and synthesis of sγPNA-based anti-miR-141-3p probes

Our prior study in C57BL/6 mice showed persistently elevated miR-141-3p levels for 2 weeks after stroke.[12] In this study, we designed sγPNA sequences complementary to target miR-141-3p

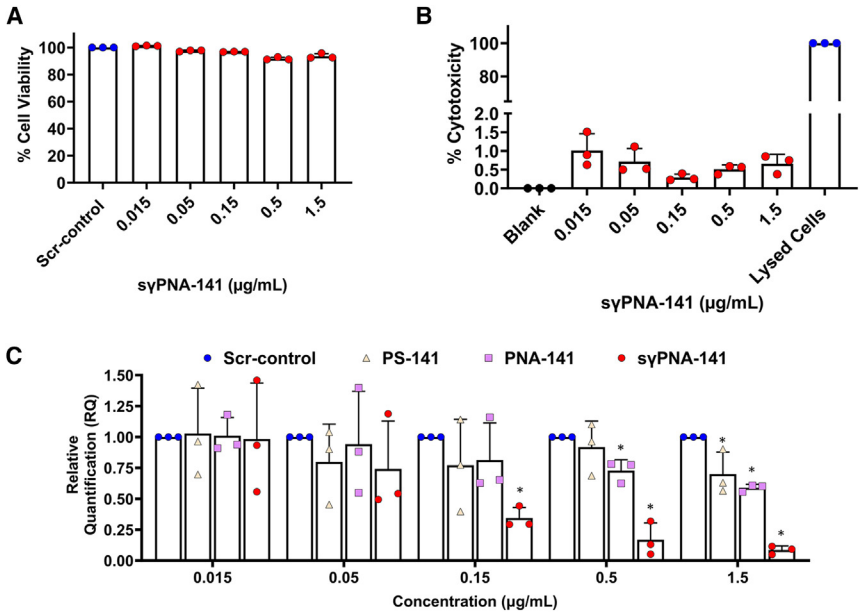

Figure 2. *In vitro* safety and efficacy assessment of sγPNA-141 NPs in HEK293 cells

(A) Dose-dependent effect of sγPNA-141 on MTT cell viability assay and (B) Lactate dehydrase cellular toxicity assay. Data suggest that NPs with sγPNA-141 are highly tolerable with no apparent toxicity across a dose range of 0.015–1.5 μg/mL. (C) A relative miR-141-3p gene expression analysis in the RNA isolated from HEK293 cells after 24 h exposure to different concentrations of PS-141, PNA-141, and sγPNA-141 NPs. Three individual experiments were performed using different passage HEK293 cells. Data are presented as mean ± SD (*$p < 0.05$ vs. scr-control).

(Figures 1A and 1B). We synthesized sγPNA-141 using Boc-based solid-phase synthesis protocols.[24,25] Furthermore, quality control assessment of these PNAs was performed using reverse-phase HPLC and mass spectrometry analysis. Scrambled PNA oligomers were used as controls (scr-sγPNA).

Formulating and characterizing PLGA NPs

In prior studies, we determined that acid-terminated and ester-terminated PLGA NPs (consisting only of poly-lactic acid and poly-glycolic acid in an equal ratio, 50% of each) can effectively deliver PS- and PNA-based anti-miRs.[26,27] In this study, we sought to develop NP formulations that encapsulate and deliver the optimum amount of sγPNA-based anti-miR-141 and their respective scrambled controls. The hydrodynamic diameter, polydispersity index (PDI), and surface charge of NPs was determined by dynamic light scattering studies (DLS). The hydrodynamic diameter of the sγPNA-141 NPs was found to be 170 nm (Figure 1C). The formulated NPs had a narrow PDI ranging between 0.10 and 0.15 (Figure 1D) and had a zeta potential of −20 to −15 mV (Figure 1E).

sγPNA-141 loading and nucleic acid release profile

We confirmed the loading of sγPNA-141 into PLGA NPs using an organic solvent extraction method and observed an average loading of ∼300 pmol/mg for sγPNA-141 NPs (Figure 1F). These loading results suggest that sγPNA anti-miRs can be effectively encapsulated in PLGA NPs using the double emulsion solvent evaporation technique.[28,29] We further calculated the nucleic acid release profile from the PLGA NPs by re-suspending them in phosphate-buffered saline (PBS) and measuring the UV-vis absorbance at 260 nm at various time points (Figure 1G). We found maximum anti-miR release occurred within 30 min followed by sustained release of up to 8 h. This demonstrates that sγPNA-141 can effectively load and release from the NPs without any interference from the polymer.

In vitro safety analysis of sγPNA-141

We next evaluated the safety of sγPNA-141 in HEK293 cells. HEK293 cells were treated with sγPNA-141 at concentrations ranging from 0.015 to 1.5 μg/mL for 24 h. Cell viability and cytotoxicity were assessed using an MTT (3-[4,5-dimethylthiazol-2-yl]-2,5 diphenyltetrazolium bromide) assay and a lactate dehydrogenase (LDH) release assay, respectively. As expected, we did not observe cytotoxicity for sγPNA-141 at all the indicated doses (Figures 2A and 2B). These results suggest that the sγPNA-141 has no adverse effects at cellular level and is well tolerated.

Efficacy testing of sγPNA-141 at different doses *in vitro*

To compare the efficacy of sγPNA-141 to other miR-141-3p inhibitors, we also used PS-based and regular PNA-based miR-141-3p inhibitors encapsulated in PLGA NPs (PS-141 and PNA-141). HEK293 cells were treated with PS-141, PNA-141, and sγPNA-141 at concentrations ranging from 0.015 to 1.5 μg/mL. After 24 h, total RNA (including miRs) was isolated from the exposed cells and miR-141-3p expression was measured by qPCR. Our results suggest that sγPNA-141 shows higher efficacy in inhibiting miR-141-3p compared with PS-141 and PNA-141 in the treated HEK293 cells (Figure 2C). Further analysis suggests that the estimated IC_{50}[30] of sγPNA-141 (0.02 μM) is the lowest among all the tested inhibitors (0.43 μM for PS-141 and 0.25 μM for PNA-141) suggesting that sγPNA-141 is the most potent inhibitor (Figure S2).

Plasma miR-141-3p levels increase progressively after ischemic stroke in human stroke subjects

Previous studies from our lab identified miR-141-3p as a unique, progressively upregulated miR in a mouse model of stroke.[12] To validate miR-141-3p as a potential therapeutic target for stroke in clinics and translational settings, we measured the miR-141-3p levels in plasma samples of age-matched healthy control and stroke subjects at acute (day 3 ± 2) and chronic (day 65 ± 20) time points. Consistent with preclinical data, we found a progressive increase ($p = 0.0355$) in

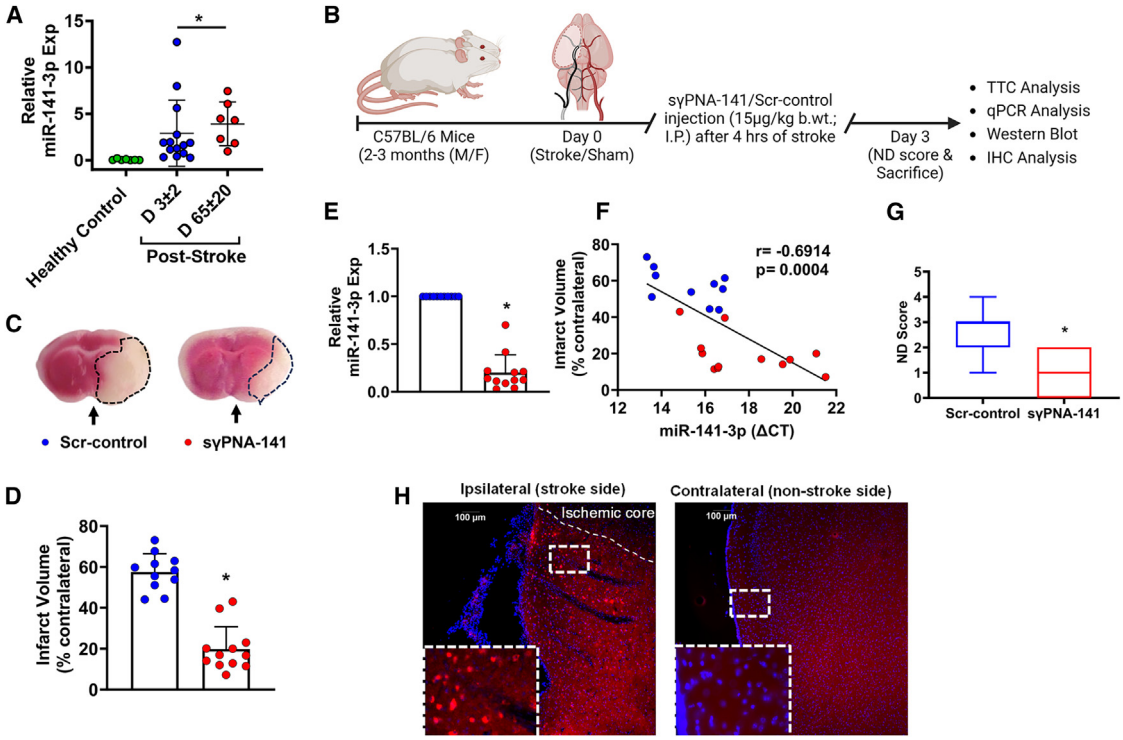

Figure 3. Expression of miR-141-3p in stroke subjects and acute neuroprotective effects of sγPNA-141 treatment in an *in vivo* mouse model of ischemic stroke

(A) miR-141-3p expression levels in plasma samples acquired from aged-matched (58–90 years) healthy control (n = 11) and stroke subjects (n = 11) from acute and chronic time points. Data are mean ± SD (*p < 0.05 vs. healthy control). (B) Schematic representation of the acute cohort experimental setup. (C) The representative images show the changes in the infarct injury after the sγPNA-141 treatment in post-stroke mice. (D) Quantitative analysis of infarct volume compared with scr-control (*p < 0.05 vs. scr-control, t test) after a single intraperitoneal injection (15 μg/kg b.wt. of sγPNA-141) given 4 h after onset of MCAo (n = 11 scr-control and n = 12 sγPNA-141). (E) sγPNA-141 treatment reduced relative miR-141-3p gene expression as revealed by analysis of RNA isolated from the perilesional cortex of mice after ischemic stroke (n = 6 mice per group) (*p < 0.05 vs. scr-control, t test). (F) Correlation analysis showed significant correlation between miR-141-3p expression and infarct volume after stroke. (G) sγPNA-141 treatment also improves the neurological deficit score (n = 22 scr-control and n = 27 sγPNA-141) (*p < 0.05 vs. scr-control). Each dot represents an individual sample. Data are mean ± SD. (H). *In vivo* biodistribution of TAMRA-tagged NPs of sγPNA-141 after intraperitoneal injection (70 h after stroke onset, i.e., 2 h before sacrifice) in mice at 3 days (72 h after stroke in the paraformaldehyde fixed coronal brain slice. Blue (nucleus; DAPI), red, -TAMRA-tagged NPs of sγPNA-141). Scale bar, 100 μm.

miR-141-3p levels in plasma samples of stroke patients (Figure 3A). These data suggest that miR-141-3p can be a potential drug target in clinical stroke subjects.

sγPNA-141 post-stroke reduces stroke injury in a mouse model of ischemic stroke

We evaluated the *in vivo* efficacy of miR-141-3p inhibitor sγPNA-141 and its scramble control (scr-control) in a transient MCAo model of ischemic stroke (Figure 3B). A single intraperitoneal (i.p.) injection (15 μg/kg b.wt. 4 h after MCAo) of sγPNA-141 significantly (p < 0.0001 vs. scr-control) reduced infarct volume at 3 days after stroke (Figures 3C and 3D). We also performed qPCR analysis of miR-141-3p using total RNA isolated from the perilesional ipsilateral cortex tissue of both scr-control- and sγPNA-141-treated groups. We found that sγPNA-141 reduced the miR-141-3p expression by ∼5-fold compared with scr-control (p < 0.0001) (Figure 3E). Our results indicated the high efficacy of sγPNA-141 in inhibiting miR-141-3p levels in brain tissue. Given the stroke is sexually dimorphic disorder, we also show neuroprotection data of sγPNA-141 in both male and female mice separately, but we did not see sex in response of the treatment (Figure S3). Therefore, we did not do separate analysis in any further experiments. Furthermore, correlation data revealed that brain tissues with lower miR-141-3p levels had significantly reduced infarct volume (r = 0.9235; p = 0.0085), indicating that miR-141-3p is directly involved in stroke injury (Figure 3F). Consistent with these observations, sγPNA-141-treated group showed a significant improvement in the neurological deficit (ND) score at 3 days after stroke (p < 0.0001 vs. scr-control) (Figure 3G). sγPNA-141 is highly specific for miR-141-3p as it did not decrease the level of other miRNAs such as miR-181c or miR-124 (Figure S4A). Furthermore, a single dose of sγPNA-141 can reduce miR-141-3p expression up to 15 days after stroke (p < 0.0001 vs. scr-control) (Figure S4B). These data suggest that sγPNA-141 post-treatment is highly specific and efficacious in reducing stroke injury.

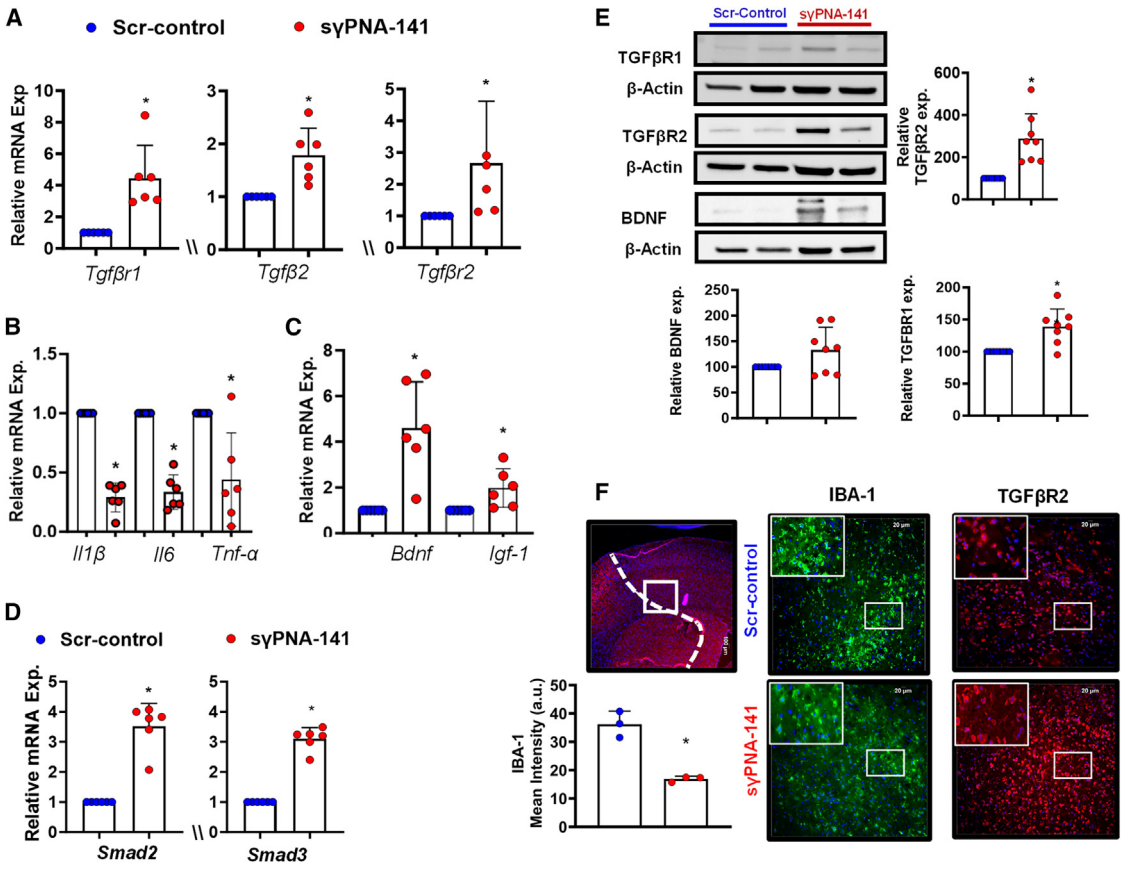

Figure 4. Effect of sγPNA-141 treatment on its direct and indirect targets

Using perilesional ipsilateral brain tissue taken from mice reperfused for 3 days post-stroke, we isolated total RNA and protein and used paraformaldehyde-fixed coronal brain sections to validate the effect of miR-141-3p inhibition by syPNA-141 *in vivo*. (A) Direct target genes like *Tgfβ2*, *Tgfβr1*, and *Tgfβr2* were increased after sγPNA-141 treatment. (B) sγPNA-141 also reduced proinflammatory mRNA like *Il-1β*, *Il-6*, and *Tnfα* and (C) increased *Bdnf* (a direct target) and *Igf-1* levels. (D) sγPNA-141 treatment also increased the expression of mRNA for *Smad2* and *Smad3*, which are the downstream targets of TGF-β family proteins. Each dot represents an individual sample ($n = 6$ mice per group) (*$p < 0.05$ vs. scr-control, t test). (E) Western blot analysis of TGF-βR1, TGF-βR2, and BDNF (28kd pro-BDNF) further confirm sγPNA-141 de-represses the effect of miR-141-3p on the translation of these proteins (n = 3–4 mice per group). (F) Immunofluorescence images show increased TGF-βR2 expression, which corroborated our qPCR and western blot data. The reduced IBA-1 expression in the sγPNA-141-treated group, confirming that sγPNA-141 reduced neuroinflammation after stroke. Dara are meanSD. Scale bars, 100 and 20 μm.

sγPNA-141 treatment upregulates miR-141-3p target genes and proteins in brain tissue

To observe the effect of sγPNA-141 treatment on miR-141-3p′s mRNA targets, we measured the mRNA levels of transforming growth factor β (TGF-β) pathway genes (such as *Tgfβ2*, *Tgfβr1*, and *Tgfβr2*) that have binding sites for the seed sequences of miR-141-3p (Figure S5) at 3 days after stroke. miRs repress the expression of mRNA targets by promoting translational repression and mRNA degradation. Thus, blocking miR-141-3p with sγPNA-141 should up-regulate miR-141-3p′s direct mRNA targets. In addition to assaying direct mRNA targets, we also analyzed the effect of anti-miR-141-3p therapy on downstream effector genes of the Tgfβ pathway family (e.g., *Smad 2* and *Smad 3*). We found sγPNA-141 treatment significantly increased ($p < 0.05$ vs. scr-control) the expression of *Tgfβ2*, *Tgfβr1*, *Tgfβr2*, *Smad2*, and *Smad3* mRNA levels (Figures 4A and 4B). Consistently, we found significant upregulation of TGF-βR1 and TGF-βR2 proteins in the brain tissue of sγPNA-141-treated mice after stroke (Figures 4E and 4F). Overall, this data suggested that sγPNA-141 treatment provides neuroprotective effects mediated by the TGF-β pathway proteins after stroke. Other direct targets of miR-141-3p, including *Sirt1*, *Cxcl12*, *Pdcd4*, *Pten*, and *Slc23a2*, were upregulated in perilesional ipsilateral brain tissue of mice treated with sγPNA-141 after stroke (Figure S6).

sγPNA-141 treatment reduces proinflammatory gene expression and increases expression of cell growth factors

sγPNA-141 treatment significantly downregulated miR-141-3p and upregulated miR-141-3p′s target genes and reduced the infarct volume in the acute phase post-stroke. To identify the mechanism of

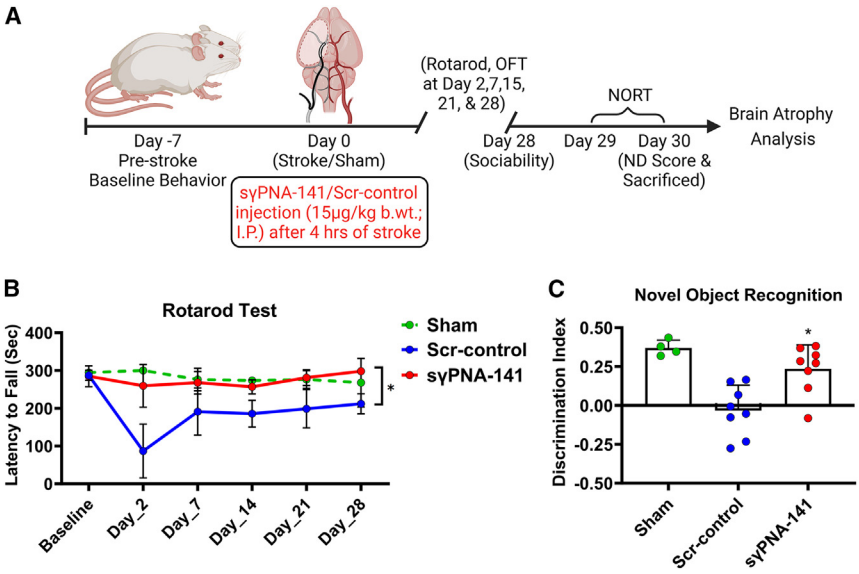

Figure 5. Effect of sγPNA-141 treatment on motor coordination and memory task during post-stroke chronic recovery

(A) Schematic representation of the chronic cohort experimental setup and timeline. (B) sγPNA-141 treatment significantly improved long-term sensorimotor recovery as revealed by a reduced latency to fall in a rotarod test (two-way ANOVA compared mean of the row F (5, 78) = 13.84. ordinary alpha $p < 0.05$ vs. scr-control). (C) Learning and memory deficits were improved after sγPNA-141 treatment as shown by the reversal in discriminating index using novel object recognition task (*$p < 0.05$ vs. scr-control one-way ANOVA multiple comparison test). Data are mean ± SD. Each dot represents an individual sample ($n = 4$ sham, $n = 7$ scr-control, and $n = 8$ sγPNA-141).

neuroprotection, we further analyzed mRNA of several proinflammatory genes (*Il-1β*, *Il-6*, and *Tnfα*) and pro-survival growth factor genes such as *Bdnf* and insulin-like growth factor-1 (*Igf-1*) after sγPNA-141 treatment. We found that the expression levels of *Il-1β*, *Il-6*, and *Tnfα* as measured by mRNA were significantly downregulated (Figure 4C) and levels of *Bdnf* and *Igf-1* were significantly upregulated (Figure 4D) in the sγPNA-141-treated mice. *Bdnf* mRNA has a binding site for the seed sequence of miR-141-3p, which thus makes *Bdnf* mRNA a direct target of this miR (Figure S5). The effect of sγPNA-141 treatment on the *Bdnf* gene was also confirmed on the protein level (Figure 4E). Following sγPNA-141 treatment, we observed reduced expression of IBA-1, an activated microglia/macrophage marker whose increased expression suggests increased inflammation after stroke (Figure 4F). These data suggest that miR-141-3p inhibition via sγPNA-141 can also reduce inflammation and enhance post-stroke recovery by mediating direct and indirect target proteins of miR-141-3p.

sγPNA-141 treatment improves sensorimotor function after stroke

To assess the effect of sγPNA-141 treatment on functional recovery after stroke, we subjected sγPNA-141- or scr-control-treated mice to a rotarod assessment once per week. sγPNA-141 treatment mice displayed swift recovery by showing increased grip strength during the early phase of recovery ($p = 0.0073$) (Figure 5B). These data suggest that sγPNA-141 treatment alleviated stroke-induced motor deficits and helped early recovery after ischemic stroke. However, sγPNA-141-treated mice did not show any significant change in exploratory and anxiety-like behavior measured by open field test (OFT) (Figures S7A and S7B).

Long-term sγPNA-141 treatment effect on memory and social behavior

Next, we performed the novel object recognition test (NORT) to analyze the effect of sγPNA-141 treatment on mice learning and memory before sacrifice (day 29/30 post-stroke). sγPNA-141 treatment significantly restored ($p = 0.032$) the loss in memory induced by stroke (Figure 5C). Similarly, the sγPNA-141-treated mice had an increasing trend of higher sociability, suggesting lessened depression-like behavior (Figure S7C). These data suggest that sγPNA-141 treatment improves learning and memory deficits caused by stroke.

sγPNA-141 treatment reduces brain tissue atrophy and mortality after stroke

Consistent with its reduction in infarct injury after stroke, treatment with sγPNA-141 also significantly reduced tissue loss measured 30 days after stroke ($p = 0.0357$) (Figures 6A and 6B). sγPNA-141-treated mice had a lower mortality rate ($p = 0.0349$) compared with the scr-control-treated mice after stroke (Figure 6C). In addition, sγPNA-141 treatment also improves the recovery in body weight after ischemic stroke (Figure S7D). No significant differences in the neurological deficit (ND) score were found between the treatment and control groups at the end of the chronic cohort (Figure 6D). These data suggest that sγPNA-141 can impart sustained neuroprotective effects during chronic recovery after stroke and rescue tissue loss in the penumbra after ischemic stroke.

DISCUSSION

Despite being a leading cause of disability, the treatment for ischemic stroke is limited to thrombolytic drug rt-PA and mechanical thrombectomy. Unfortunately, only 5%–13% of total stroke cases are eligible for these interventions.[31] There is not a single FDA-approved neuroprotective agent for the treatment of ischemic stroke. Recently, the significance of small noncoding endogenous RNAs, known as miRNAs (or miRs), are increasingly recognized for their ability to regulate the expression of multiple genes and the mRNA of numerous target proteins, exerting control over entire pathways.[32] Several miRNAs, such as miR-1246, miR-4516, miR-320a-3p, miR-320c, miR-204-3p, miR-17-5p, miR-16-5p, and miR-423-5p, are dysregulated in the blood or CSF samples of stroke patients.[8] These miRNAs can promote or inhibit the formation of secondary brain damage. For

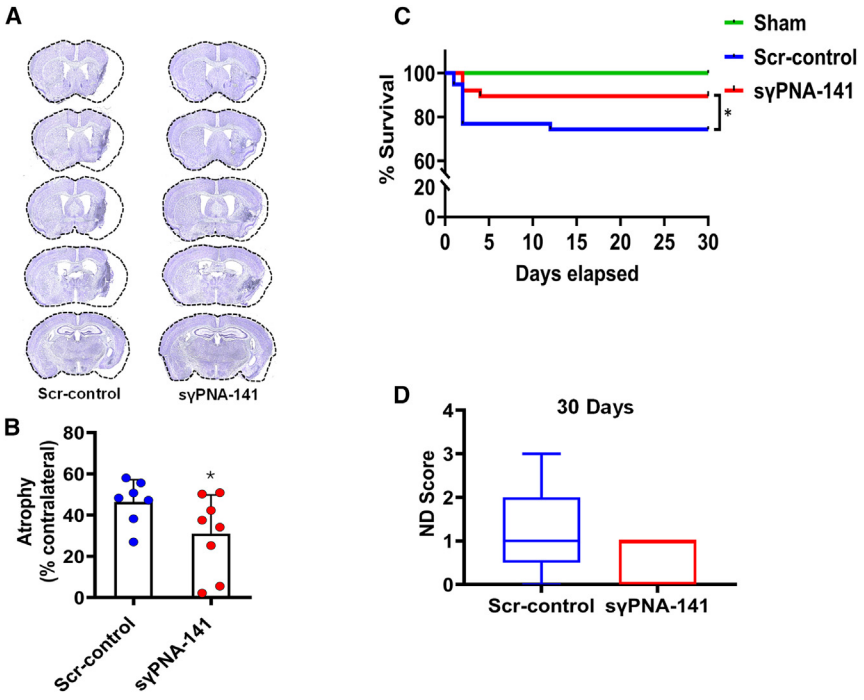

Figure 6. Effect of sγPNA-141 treatment on long-term neuroprotection, survival, and atrophy

(A) Representative cresyl-violet-stained coronal brain sections of sγPNA-141-treated mice and scr-control mice after 30 days stroke recovery. (B) Quantitative analysis show that sγPNA-141-treated mice had significantly less tissue loss compared with scr-controls (n = 7–8 mice per group). (C) Effect of sγPNA-141 on survival (n = 40–45 mice per group) and (D) ND score (n = 9–12 mice per group) after 30 days of stroke onset (*p < 0.05 vs. scr-control, t test). Data are mean ± SD. Each dot represents an individual sample.

example, they may promote neuron regeneration or apoptosis, alleviate leakage across the blood-brain barrier (BBB), disrupt intracellular transport, and decrease inflammatory response in ischemic and traumatic brain injuries.[12,33] Recently, we and others have demonstrated that miRNAs such as miR-141-3p and miR-181c are dysregulated during ischemic stroke and contribute to stroke pathophysiology.[9,12,13,34] We identified miR-141-3p as a potential therapeutic target for treating ischemic stroke in mice.[12] Our data from human stroke subjects further reiterate that miR-141-3p is a potential drug target for ischemic stroke treatment. We further reported the inhibition of miR-141-3p using commercially available (antagomiR141-3p, Ambien, Life Technologies Camarillo, CA) and PNA-based miRNA inhibitors, which mitigates damage after stroke and improves recovery.[13] In this study, we generated a novel, advanced, and efficacious sγPNA-based miR-141-3p inhibitor and compared its *in vitro* efficacy with regular PNA- and PS-based anti-miRs. For *in vivo* or *in vitro* delivery, we encapsulated these inhibitors in biocompatible PLGA-based NPs for efficient delivery. After the characterization of NPs, we tested the safety and compared the efficacy of novel sγPNA-based miR-141-3p inhibitors with regular PNA and PS in HEK293 cells. Prior cancer-based studies established that gamma PNA-based inhibitors do not exert any toxicity in the multiple mouse models.[25,35–37] Furthermore, we also tested the neuroprotective potential of sγPNA-based inhibition of miR-141-3p at the molecular and behavioral level.

One of the primary obstacles preventing the effective delivery of miR inhibitors to target cells is the instability of miR inhibitors in the bloodstream. Anti-miRs are often rapidly degraded by circulating nucleases or proteases. Unlike PS-based or regular PNAS, sγPNAs are more stable because they have a backbone highly resistant to nucleases and proteases.[38] Still, sγPNAs cannot permeate a biological barrier like the BBB, precluding uptake of sγPNA in the brain where it would bind and inhibit miRs with high specificity. To overcome this limitation, one strategy is to take advantage of the partial rupture of the BBB that occurs during the first few days after stroke injury,[39,40] which allows partial delivery of therapeutic agents like sγPNAs immediately after stroke. While potentially effective, this strategy does not enable the complete and longer-term delivery of anti-miRs after stroke. Here, we used nanoformulation approaches to deliver sγPNA-141 to enable it to cross the BBB more efficiently. While we did not directly measure whether NP encapsulation increased the brain uptake of sγPNA-based inhibitors compared with naked sγPNA inhibitors, we found that NP-encapsulated sγPNA-141 treatment reduced the expression of miR-141-3p in the brain and further showed that sγPNA-141 NPs did penetrate the brain. Beyond enabling crossing of the BBB, nanoformulation also offers several other advantages for drug delivery, such as decreased drug dose, reduced side effects, and increased drug stability,[41] and also eliminates the need for transfection reagents.[13] Our data here corroborates these observations and is consistent with our previous works showing that PLGA-based nanoformulations of brain-derived neurotrophic factor (BDNF)[39] and PNA-based miR inhibitors can efficiently cross the BBB to provide long-term therapeutic benefits after stroke.[13]

Delivery safety is a big concern for NP-based therapeutics. The size and zeta potential of PLGA NPs significantly influences resulting cytotoxicity.[42] Our results showed that sγPNA-141 containing NPs had desirable physical-biochemical properties, including uniform size, distribution, charge, release profile, and optimum loading efficiency. Furthermore, we did not observe in-vitro cytotoxicity for sγPNA-141 at all the evaluated doses. This suggests that sγPNA-141 is biocompatible and well tolerated even at higher doses in the *in vitro* settings.

Previously, we tested PS-based and regular PNA-based anti-miR-141-3p for the inhibition of miR-141-3p and established that regular PNA-141 reduced miR-141-3p expression more efficiently than

PS-141. We also confirmed that PNA-141 showed better neuroprotection at 3 days after ischemic stroke. Consistent with the high efficacy of sγPNA-based miR inhibitors in inhibiting endogenous miR levels, a sγPNA-141 inhibited miR-141-3p expression *in vitro* to a similar extent as both PS-141 and regular PNA-141 but at a much lower dose. Previously, we also showed that PNA-141 resulted in significant neuroprotective effects when delivered at a dose of 50 μg/kg b.wt. to mice subjected to ischemic stroke.[13] Compared with regular PNA-141, sγPNA-141 showed similar or better neuroprotective effects as this PNA-141 treatment but at a much lower *in vivo* dose (3-fold lower, 0.015 μg/kg b.wt.), suggesting high potency due to the efficient binding of sγPNA-141 with its target sequence on its miRNA. Systemic injection of sγPNA-141 at this low concentration reduced the infarct damage and miR-141-3p expression in brain tissue of mice subjected to stroke and improved the long-term recovery measured up to 30 days after stroke. Reduced acute inflammation, improved sensorimotor deficits, and learning and memory function during long-term recovery further support the neuroprotective and neurorehabilitation functions of sγPNA-141 after stroke.

The present data suggest that acute neuroprotection and enhanced post-stroke functional recovery affected by sγPNA-141 administration is mediated by miR-141-3p′s downstream target genes, like *Bdnf* and *Tgfβ*, or by the indirect effect of sγPNA-141 on growth factors such as *Igf-1* and inflammatory cytokines such as *Il-1β*, *Il-6*, and *Tnf-α*. The TGF-β family, including members TGF-β1, TGF-β2, and TGF-β3, plays important roles post-stroke, including regulating immune responses, cell proliferation, and neuroprotection.[43] TargetScan analysis of 3′ UTR of *Tgfβ2*, *Tgfβr1*, and *Tfgβr2* showed each gene has a binding site for miR-141-3p (Figure S5). TGF-β proteins exert their function via a tetrameric receptor complex, which is composed of two receptors, TGF-βR1 and TGF-βR2 (2 units each), both of which are highly expressed on microglia.[44] In the canonical TGF-β pathway, the assembly of these receptor complexes leads to subsequent phosphorylation of downstream Smad proteins (SMAD2/3), which are transcription regulators for target genes.[45] The *Tgf-β/Smad2/3* pathway protects from apoptotic neuronal cell death and promotes tissue regeneration in stroke mice.[46] *Tgf-β2/Tgf-βr2* axis is also involved in the NG2-mediated inhibition of microglial activation and protection from inflammation,[47] concurrent with reduced expression of IBA-1 and proinflammatory cytokines. The TGF-β family is also involved in the regulation and secretion of many cytokines, including lL-1β, IL-6, and TNF-α and other interleukins,[48] suggesting that TGF-β family member proteins might regulate reduced expression of these proinflammatory cytokines we observed in sγPNA-141-treated mice. These data bolster our observation that the neuroprotective effects of sγPNA-141 were partially mediated via reduced inflammation and other neuroprotective effects of TGF-β family proteins. Our finding that miR-141-3p remains elevated for several months in human stroke subject further confirm its role in inflammation after stroke which is consistent with prior work from multiple labs who reported chronic systemic inflammation after acute stroke injury.[49–51] Our data indicate that a reduction in miR-141-3p with sγPNA-141 results in decreased inflammation, further supporting the notion that increased expression of miR-141-3p may be responsible for sustained elevated inflammation after stroke. Therefore, its inhibition can reduce inflammation.

Bdnf and Igf1 are crucial factors for regulating neuronal growth, repair, and neuroplasticity.[52] Interestingly, Igf-1 also regulates Bdnf expression, influencing genes associated with Bdnf-related neurogenesis and contributing to the growth and differentiation of brain neuron units.[52,53] Higher expression of *Bdnf* and *Igf-1* after sγPNA-141 treatment might be another possible mechanism for improved motor and memory function. Bdnf showed a binding site for miR-141-3p, and thus, increased levels of miR-141-3p may be responsible for downregulation of Bdnf in stroke, which was reversed by its inhibition with sγPNA-141. Despite extensive work on efficacy testing with sγPNA-141, we acknowledge certain limitations of this study. We did not report the sexually dimorphic effects of sγPNA-141 on various post-stroke outcomes, except for infarct size analysis, where no sex difference in response to sγPNA-141 was observed. In addition, we did not investigate cell-specific effects or *in vivo* safety study at higher doses (beyond the therapeutic dose) of miR-141-3p in this study.

In conclusion, we have demonstrated novel miR-141-3p inhibitors sγPNA-141 are efficacious in providing neuroprotective effects and enhanced recovery after ischemic brain injury. Post-stroke sγPNA-141 treatment significantly reduced the infarct injury after stroke and increased the expression of several neuroprotective genes (*Tgfβ2*, *Tgfβr1/r2*) and growth factors (*Bdnf*, *Igf-1*) and reduced the responses of proinflammatory cytokines (*Il-1β*, *Il-6*, and *Tnf-α*). Elevation in *Smad2* and *Smad3* expression suggests Tgfβ/Smad2/3 signaling (Figure 7) is the primary mechanism of neuroprotection after sγPNA-141 treatment in mice subjected to stroke. sγPNA-141 treatment also improves long-term behavioral recovery, as revealed by several assays, including a reduction in sensorimotor deficits and improved learning and memory, demonstrating promising translational potential for ischemic stroke treatment. Overall, our data suggest miR-141-3p is a potential drug target, and inhibition of miR-141-3p using sγPNA-141 could be an effective treatment for ischemic stroke.

MATERIALS AND METHODS

sγPNA synthesis

Boc-protected serine gamma monomers were purchased from ASM Research Chemicals (Hannover, Germany) and vacuum dried for at least a week before the synthesis. About 100 mg lysine-loaded resin was soaked in dichloromethane (DCM) in the reaction vessel. The DCM was drained off after 5 h, and the resin was deprotected using trifluoroacetic acid (TFA):m-cresol (95:5) solution for 5 min. The deprotection step was repeated two additional times. The resin was thoroughly washed with DCM and N,N, dimethylformamide (DMF). The monomer was dissolved in coupling solution consisting of 0.52 mol/L di-isopropylethylamine, and 0.39 mol/L of O-benzotriazole-N,N,N′,N′-tetramethyl-uronium-hexafluoro-phosphate and

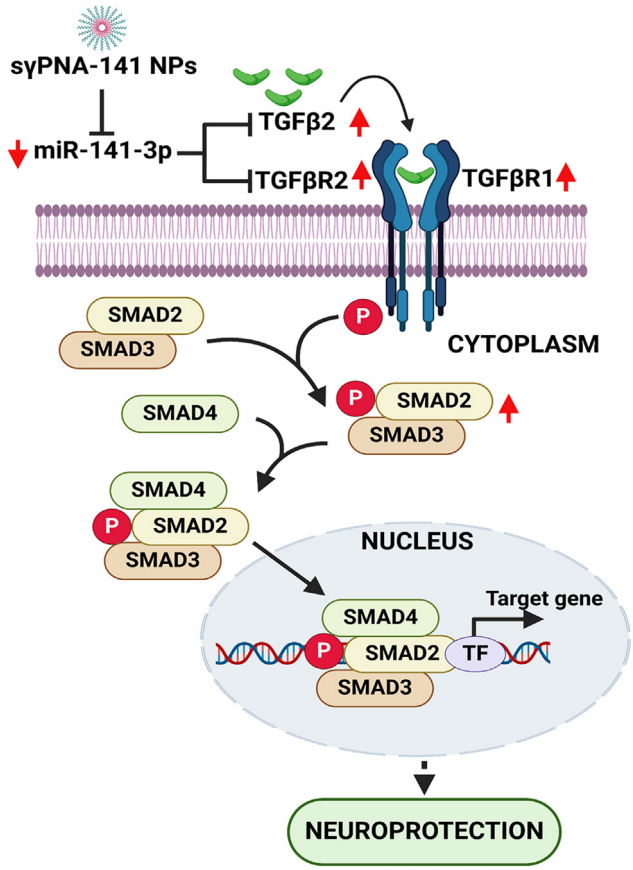

Figure 7. Schematic of the proposed mechanism by which syPNA-141 exerts its neuroprotective action

Stroke-induced upregulation of miR-141-3p in brain is reduced by syPNA-141, which increases the expression of transforming growth factor β (TGF-β) family proteins. This is followed by the phosphorylation of Smad2/3 proteins to form the Smad2/3/4 complex, which associates with transcription factors and cofactors to modulate the expression of its target genes in the nucleus.

0.2 mol/L N-methyl pyrrolidone (NMP). This coupling reaction was continued for 1.5 h followed by resin washing with DCM and DMF. The success of coupling and deprotection steps was confirmed by the Kaiser test. The capping was performed using a mixture of NMP, acetic anhydride, and pyridine, followed by resin washing with DCM. All the above steps were repeated until the last monomer was added to the reaction vessel. The PNA was cleaved from the resin using a cleavage cocktail comprising thioanisole, m-cresol, TMFSA, TFA (1:1:2:6). The PNA was collected after 1.5 h and precipitated using cold diethyl ether and then centrifuged at 3,500 rpm for 5 min. This step was repeated two additional times. The PNA was vacuum dried and purified by reverse-phase high-performance liquid chromatography (RP-HPLC, Shimadzu). The concentration of PNA was calculated by measuring the absorbance at 260 nm on the NanoDrop One (Thermo Fisher Scientific) using the extinction coefficient of individual monomers (11,700 M^{-1} cm^{-1} (G), 6,600 M^{-1} cm^{-1} (C) 13,700 M^{-1} cm^{-1} (A), 8,600 M^{-1} cm^{-1} (T)).

NP preparation

The NPs were formulated using the double emulsion solvent evaporation technique. About 40 mg of ester-terminated PLGA polymer was dissolved in 0.5 mL DCM. Forty nanomoles of PNA was introduced dropwise to the PLGA DCM solution with continuous stirring and then probe sonicated (10 s × 3 cycles) to form oil-in-water (o/w) primary emulsion. This o/w emulsion was added dropwise to 1 mL of 5% w/v PVA solution with continuous stirring followed by probe sonication (10 s × 3 cycles) to form water in oil-in-water (w/o/w) double emulsion. This double emulsion was then added to 10 mL 0.3% w/v PVA solution with continuous stirring and left overnight for the DCM to evaporate. The NPs were washed with cold water by centrifuging at 9,500 rpm for 10 min at 4°C to remove the excess PVA. This washing step was repeated two additional times. The NPs were redispersed in 5 mg/mL trehalose solution and then freeze dried.

DLS

The NP samples ($n = 3$) were dispersed in 1,000 μL of water and subjected to brief vortexing. The NP suspension was then analyzed by the Zetasizer Nano ZS (Westborough, MA) to assess the zeta potential, PDI, and hydrodynamic diameter of the NPs.

Loading study

DCM (200 μL) was introduced to the NPs and the mixture was agitated for 3 h at a speed of 1,000 rpm. Subsequently, 200 μL of 1× TE buffer was incorporated into the NPs, and the agitation continued for an additional 3 h at 1,000 rpm. Following this, the NPs were centrifuged at 15,000 rpm at 4°C. The absorbance of the resulting supernatant was assessed at 260 nm using NanoDrop One.

Nucleic acid release profile

About 2 mg of NPs were weighed in an Eppendorf tube. The NPs were dispersed in 0.3 mL PBS and agitated at 300 rpm at 37°C. Samples were withdrawn at 0.5, 1, 2, 4, 6, 8, 12, and 24 h time points by centrifuging the NP tube at 15,000 rpm for 10 min at 4°C. The supernatant from the centrifuged NP tubes was gently removed without disturbing the sedimented NP pellet, and absorbance of the supernatant solution was measured at 260 nm wavelength using NanoDrop One (Thermo Fisher Scientific, Waltham, MA). The NP pellet was redispersed in 0.3 mL fresh PBS and agitated at 300 rpm at 37°C until the next time point. NP samples from three different batches were used for the release study.

Clinical sample procurement and time points

The clinical plasma samples of both de-identified stroke and healthy control subjects were obtained from the UConn Health Research Biorepository. These data consisted of de-identified plasma samples collected at 3 points (day 1, day 2–5, and day 30+) from total 11 stroke subjects. We combined time point 1 and time point 2 to represent acute time points (day 3 ± 2). The demographic details are given in supplementary file (Table S2).

Cell culture, NP exposure, cell viability, and cytotoxicity

HEK293 cells obtained from ATCC (Manassas, VA) were maintained in a DMEM medium containing 1% antibiotic/antimycotic (Ab/Am) solution and 10% fetal bovine serum. The cells were cultivated at a temperature of 37°C in an environment consisting of 5% CO_2 and 95% relative humidity. Cell viability assay was performed using MTT reagent (cat. no. 475989, Sigma-Aldrich) per manufacturer protocol. In brief, an equal number of cells (10,000 cells) were seeded in 96 well plates and cultured overnight. Cells were exposed to scrambled control, PS, regular PNA, and sγPNA-141 at various concentrations ranging from 0.015 to 1.5 μg/mL for 24 h. Following a single wash, the cells were incubated in 100 μL of serum-free media with 0.5 mg/mL MTT at 37°C for 2 h. About 100 μL of HCL was added to each well. This solution was mixed with a pipette and then incubated for 60 min at 37°C. The absorbance was measured at 570 nm in a plate reader. A cytotoxicity assay was performed by CyQUANT LDH Cytotoxicity Assay (cat. no. C20300) as per manufacturer protocol. An equal number of cells (10,000 cells) were seeded in 96-well plates and incubated overnight. In triplicate, one of the following was added to each well: sterile water (spontaneous LDH activity), 10× lysis buffer (maximum LDH activity), and various concentrations of sγPNA-141 ranging from 0.015 to 1.5 μg/mL (compound-treated LDH activity) for 24 h. Each solution was incubated with cells for 45 min in a cell incubator (37°C, 5% CO_2). Media (50 μL) from each well was transferred to new 96-well plates, and an equal volume of the cytotoxicity reaction mixture was added to each well. Plates were incubated for 30 min at room temperature. To stop the reaction, 50 μL of stop solution was added to each well and absorbance was measured at 490 nm. Percentage cytotoxicity was calculated by the following formula:

$$\%\text{cytotoxicity} = (\text{compound-treated LDH activity} - \text{spontaneous LDH activity/maximum LDH activity} - \text{spontaneous LDH activity}) \times 100.$$

Experimental animals

All mice (C57BL/6, male and female, 2–3 months old) were obtained from Jackson Laboratory (Bar Harbor, ME). All mice were kept at ambient temperature and humidity with *ad libitum* pellet diet and water. All experiments were performed according to protocols approved by the Institutional Animal Care and Use Committee (IACUC) at UConn Health. We followed ARRIVE Guidelines in reporting animal data.

Experimental design

In this study, we induced ischemic stroke in mice by occluding the right middle cerebral artery (MCAo) for 60 min, followed by reperfusion periods of either 3 days (to study acute effects) or 30 days (for chronic outcomes) (Figures 3A and 5A). A total of 73 C57B/6 mice (38 males and 35 females) were randomly allocated into two groups: the control group receiving scrambled PNA control, or the treatment group receiving NP-encapsulated sγPNA-141 (15 μg/kg anti-miR-141-3p:body weight, administered via i.p. injection 4 h after the onset of MCAo). Post-stroke, mice in the acute phase group were euthanized for a range of biochemical and histological examinations. Meanwhile, those in the chronic phase group underwent neurobehavioral assessments on days 2, 7, 14, 21, and 28, utilizing rotarod and OFTs, along with a novel object recognition task for memory conducted on day 29. The distribution of mice across these groups and their specific usage and mortality and exclusion are reported in Table S3. For further analysis, mice in the chronic group were prepared for brain atrophy evaluation using paraformaldehyde perfusion fixation. In contrast, mice in the acute group underwent either fixation or flash freezing for assorted assays, as outlined in Table S3. Our selection of 3 and 30 days post-stroke as analysis time points aligns with our focus on acute outcomes, characterized by peak post-stroke inflammation, and long-term chronic recovery, which holds translational significance.

MCAo

We induced transient focal cerebral ischemia by occluding the right MCAo for 60 min, a method consistent with previous studies.[10,11] The isofluorane-anesthetized (5% for induction and 1.5% for maintenance) animals underwent a ventral midline incision. We then made an incision in the right external carotid artery and inserted a 6.0 silicone-coated nylon filament (602134Re and 602234Re, Doccol, Sharon, MA) through the external carotid artery stump, extending from the internal carotid artery bifurcation. Throughout the procedure, we maintained mice temperature at approximately 37°C using heating pads, ensuring stable body temperature. Laser Doppler was used to assess successful occlusion; occlusion was considered successful if blood flow in the middle cerebral artery region was decreased to below 15% of baseline. After 60 min of occlusion, reperfusion was initiated for either 3 days (acute cohort) or 30 days (chronic cohort) based on the experimental design. Post-surgery, mice were provided with a Nutra-gel wet complete nutrition diet (Bio-Serve) for 1 week or until sacrifice (whichever is earlier) to ensure proper nutrition during chronic recovery. In addition, all mice received daily subcutaneous injections of 1 mL normal saline for hydration. For sham mice, we performed identical surgical procedures but did not insert the suture into the internal carotid artery.

Preparation of sγPNA for systemic administration

The sγPNA-141 or scr-sγPNA-141 (lyophilized powder provided by Bahal lab) were reconstituted in 1× PBS by vortexing and sonication. The solution was freshly prepared just before the i.p. administration.

TTC staining for infarct analysis

2,3,5-Triphenyl tetrazolium chloride (TTC) from Millipore Sigma (cat. no. T8877, Burlington, MA) was used for the infarct analysis. Three days after the onset of MCAo (acute cohort), all mice designated for the analysis of infarct volume were deeply anesthetized using a single injection of Avertin (250 mg/kg b.wt., i.p.) and underwent intracardiac perfusion with 40 mL of ice-cold 1× PBS to eliminate blood from their circulation. The intact whole brain was subsequently extracted and preserved at −20°C before slicing. Following a brief warming for approximately 2 min at room temperature, the brain

was cut into 5 coronal slices at 2 mm intervals. Under cold conditions, a small prelesional brain tissue from slice 3 was isolated for miR and RNA analyses. These individual brain sections were immersed in a 1.5% TTC solution (in 1× PBS at pH 7.4) for a 20-min duration at 37°C within an incubator kept in darkness. The slices were gently agitated and flipped to ensure consistent exposure to TTC staining across all surfaces. Subsequently, after a 20-min period, all the TTC was removed, and the brain slices were immersed in a 10% formalin solution until imaging. The determination of the infarct volume in each brain was carried out in a blinded manner, employing SigmaScan (version Pro 5) image analysis software. The infarct volume was computed using Swanson's method to correct for edema as described previously.[13] The total volumes of both the ipsilateral and contralateral hemispheres in both brain hemispheres were quantified, and the percentage infarct volume was calculated as a percentage of the contralateral hemisphere to prevent any potential errors due to edema.

Cresyl violet staining for tissue atrophy analysis

Tissue atrophy was measured in brains of mice from the chronic cohort (30 days after stroke) as described previously.[54] In brief, we euthanized the mice by administering a single overdose of Avertin (250 mg/kg b.wt.) intraperitoneally. Subsequently, trans-cardiac perfusion was conducted on the mice using cold PBS, followed by a 4% paraformaldehyde solution. The intact brain was isolated and fixed overnight at 4°C. The brain was transferred into the cryoprotectant (30% sucrose) for dehydration and stored at 4°C until it sank. The brains were meticulously sectioned into 30μm-thick free-floating slices using a freezing microtome. From this collection of slices, every eighth one was chosen for further processing, which involved mounting and staining with cresyl violet. These 30 μm sections were then utilized for tissue atrophy calculations, as described previously.[54] The tissue atrophy in each brain was carried out using SigmaScan (version Pro 5) image analysis software. An Investigator blinded to the experimental group analyzed the data.

Immunohistochemical analysis

Immunohistochemical staining was performed in 10 μm brain sections of acute cohort mice using a standard protocol as described previously.[55] In brief, tissue sections were mounted on Superfrost Plus charged slides (Thermo Fisher Scientific) and left for 30 min to dry. The mounted tissue sections were initially rinsed thoroughly in 0.1 M PBS. Subsequently, we conducted antigen retrieval by heating the tissue in a 10 mM sodium citrate buffer at pH 6.2 following the rinsing process. The tissue sections were then placed in a blocking solution (0.3% Triton X- and 5% normal donkey serum in 0.1 M PBS) and were allowed to incubate for 1 h. After the blocking step, the sections were incubated overnight at 4°C with the primary antibodies (IBA-1 [cat. no. MA5-27726, Thermo Fisher Scientific] at 1:200 dilution, TGFBR2 [cat. no. 66636-1-Ig, Proteintech] at a 1:200 dilution). After primary antibody incubation, tissue sections underwent rinsing with PBST (0.05% Tween 20 in 1× PBS) and were then incubated with the Alexa Fluor-conjugated secondary antibody (1:1,000) at room temperature for 1 h. Following the PBST rinse, the sections were cover slipped after addition of a drop of UltraCruz Mounting (Santa Cruz Biotech, cat. no. SC-24941) and used for imaging.

Neurobehavioral tests

We performed ND score to assess gross neurological deficits in mice. The OFT and rotarod test were used to measure spontaneous locomotory activity/anxiety-like behavior and motor activity, respectively. These neurobehavior tests were performed before the stroke surgery (baseline) and post-surgery on days 2, 7, 14, 21, and 28 as described previously.[55] To assay depression-like behavior and memory, we used sociability and NORT, respectively.

ND score

ND scores ranging from 0 to 4 were recorded at 3 and 30 days after stroke as described previously.[56] In brief, the standard scoring system was followed: 0, no deficit; 1, forelimb weakness and torso turning to the ipsilateral side when held by the tail; 2, circling to affected side; 3, unable to bear weight on affected side; and 4, no spontaneous locomotor activity or barrel rolling. Highest score by any given mouse was plotted on the y axis.

OFT

OFT is a commonly used method for assessing exploratory behavior and overall activity in rodents. In brief, mice were placed in a corner of a transparent acrylic chamber (16″ × 16″) and monitored for 10 min. The locomotor activity was calculated as total beam breaks using the photobeam activity system (San Diego Instruments, CA). To assess anxiety-like behavior, we calculated the percentage of beam breaks occurring in the center zone (16/3″ × 16/3″) relative to the total beam breaks. OFT testing can be used repeatedly to observe patterns without being impeded by habituation.[57]

Rotarod test

Sensorimotor deficits in stroke mice were measured by the rotarod task. Mice were placed on a rotating rod accelerating from 4 to 40 rpm for a period of 5 min. Each mouse was subjected to two trials, with at least a 30-min interval between the trials. We recorded the time it took for each subject to fall from the rotating rod during each trial and the mean latency was calculated for group comparisons.[58]

Sociability test

A three-chambered social interaction test or sociability was used to study post-stroke depression in mice in this study, as described earlier.[54] In brief, the apparatus consists of a rectangular, three-chambered Plexiglas box with walls that have small openings allowing access to each chamber (right, middle, and left). The social interaction test has two phases: (1) habituation and (2) testing. In the habituation phase, two wire mesh cages were kept at both ends of the chambers and a mouse was allowed to explore the chamber for a period of 5 min. Following habituation, the test mouse was returned to his home cage and a stranger mouse of same sex was placed under a round wire cage within the right chamber of the testing apparatus. Subsequently, the test mouse was reintroduced into the middle

chamber and allowed to explore the apparatus for 10 min. An observer blinded to the treatment recorded the time the test mouse spent in the chamber of the stranger mouse (right chamber). Data are presented as mean ± standard deviation (SD) of the percent of time spent in the right chamber (the chamber with the stranger mouse) relative to the total interaction time.[54]

NORT

NORT is a valuable tool for assessing cognition and recognition memory in rodent models.[39] This test capitalizes on the natural tendency of mice to devote more time to exploring a novel object compared with a familiar one, indicating intact recognition memory. In the initial phase, animals were given the opportunity to explore an empty arena for a minimum of 10 min. Subsequently, 24 h after the habituation phase, the animals encountered a familiar arena containing two identical objects that were placed in the bottom left and upper right corners of the chamber for a duration of 10 min. In the subsequent experimental trial, which occurred on the following day, the mice explored the open field in the presence of both a familiar object and a novel object. The time spent exploring each object was meticulously recorded, and the discrimination index (DI) was computed using the formula DI = (TN − TF)/(TN + TF), where TN represents the time spent exploring the novel object, and TF represents the time spent exploring the familiar objects.

RNA isolation, cDNA synthesis, and real-time PCR

Total RNA (including small RNA) was isolated from human plasma samples using miRNeasy Serum/Plasma Kit (cat. no. 217184, QIAGEN, Germany) as per manufacturer protocol. Total RNA from the HEK293 cell line used in *in vitro* experiments and from perilesional brain tissue from mice subjected to stroke was extracted using a TRIzol or miRVana miRNA isolation kit (Ambion Life Technology), respectively, per manufacturer protocol. The cDNA was synthesized for miRNA and normal gene using TaqMan MicroRNA Reverse Transcription Kit (cat. no. 4366596, Thermo Fisher Scientific) and iScript cDNA Synthesis Kit (cat. no. 1708891, Bio-R), respectively, per manufacturer protocol. TaqMan single-tube assay primers for miR-141-3p (no. 000463), U6 snRNA (no. 001973), and RNU48 (no. 001006), and other mRNAs such as *Tgfβ2* (no. Mm00436955_m1), *Tgfβr1* (no. Mm00436964_m1), *Tgfβr2* (no. Mm03024091_m1), *Smad2* (no. Mm00487530_m1), *Smad3* (no. Mm01170760_m1), *Il-1β* (no. 00434228), *Il-6* (no. Mm00446190_m1), *Tnf-α* (no. Mm00443258_m1), *Bdnf* (no. Mm04 230607_s1), *Igf-1* (no. Mm00439560_m1), *Sirt1* (no. Mm01168521_ m1), *Cxcl12* (no. Mm00445553_m1), *Pdcd4* (no. Mm01266062_ m1), *Slc23a2* (no. Mm00497751_m1), *Stat5b* (no. Mm00839 889_m1), *Pten* (no. Mm00477208_m1), *Tgfβ1* (no. Mm01178820_ m1), and *Gapdh* (no. Mm99999915_g1) were procured from Thermo Fisher Scientific. TaqMan universal PCR master mix II, no UNG (cat. no. 4440040) was procured from Thermo Fisher Scientific. Relative quantification of gene expression was done using the comparative Ct method ($2^{-\Delta\Delta Ct}$) with RNU48/U6 snRNA and *Gapdh* as normalization controls for miRNA and mRNA genes, respectively.

Target identification of miR-141-3p

miRTarBase 9.0 (https://www.mirtarbase.cuhk.edu.cn/~miRTarBase) and TargetScan Human release 7.2 web portal (http://www.targetscan.org/vert_72/) were used to identify the potential targets of miR-141-3p.[59,60]

Western blot analysis for protein

After 3 days of post-stroke treatment with sγPNA-141/scr-control, mice were euthanized with a high dose of Avertin (250 mg/kg b.wt., i.p.) followed by trans-cardiac perfusion using cold PBS. The intact brain was removed and perilesional cortical tissue from the right (ischemic) hemisphere was isolated. The tissue was homogenized in RIPA buffer supplemented with protease inhibitor and centrifuged as described previously.[61] The protein concentration was estimated by Pierce BCA protein assay kit from Thermo Fisher Scientific (cat. no. 23225). Protein (20 μg) from each sample was loaded into each well of 4%–15% polyacrylamide gels (Bio-Rad, CA) and transferred to PVDF membranes (Bio-Rad). Membranes were incubated with primary antibodies overnight (Anti-TGFβR1 [1:500, cat. no. SAB570065, Sigma-Aldrich], TGFβR2 [1:2,000, cat. no. 66636-1-Ig, Proteintech], BDNF [1:1,000, cat. no. 25699-1-AP, Proteintech]) followed by incubation with HRP-linked secondary antibody. Chemiluminescent HRP substrate was used for developing the blot and β-actin (1: 3,000, cat. no. MA5-15739, Thermo Fisher Scientific) was probed as loading control.

Statistical analysis

All data were presented as mean ± SD. GraphPad Prism 9 (San Diego, CA) was used for the statistical analysis and graph plot. Student's t tests were used to calculate statistical significance between two groups while more than two groups were analyzed by using one-way ANOVA with a Bonferroni post hoc test to correct for multiple comparisons. Owing to the ordinal nature of ND scores, the Mann-Whitney U test was used for ND score analysis. For survival curve analysis, we used log rank (Mantel-Cox) analysis to determine statistical significance between the groups. The probability value of $p < 0.05$ was considered statistically significant. An investigator blinded to the experimental groups carried out the behavioral experiments and final data analyses of all the experiments. Experimenters were not blinded for biochemical experiments.

DATA AND CODE AVAILABILITY

Data can be made available upon request of the corresponding author.

ACKNOWLEDGMENTS

This work was supported by NIH, United States (1R21NS114981) and REP Convergence (OVPR UConn, United States) grant to R.V. and R.B. We acknowledge Bernard L. Cook III, PhD, a Science Editor & Illustrator at UConn Health, for providing editorial input on the revision of this manuscript.

AUTHOR CONTRIBUTIONS

R.V. and R.B conceptualized the project and supervised *in vivo*/*in vitro* work and sγPNA-141 synthesis work, respectively. S.K.Y., K.D., D.G.T., M.-K.C., A.K.Y., and M.P. conducted experiments and analysis. R.V. and S.K.Y. carried out surgeries. S.K.Y., R.V., and R.B. drafted the manuscript. All authors reviewed the article.

DECLARATION OF INTERESTS

The authors declare no competing interests except a US patent is pending for the role of sγPNA-141 in the treatment of ischemic stroke.

SUPPLEMENTAL INFORMATION

Supplemental information can be found online at https://doi.org/10.1016/j.omtn.2024.102355.

REFERENCES

1. Feigin, V.L., Stark, B.A., Johnson, C.O., Roth, G.A., Bisignano, C., Abady, G.G., Abbasifard, M., Abbasi-Kangevari, M., Abd-Allah, F., Abedi, V., and Abualhasan, A. (2021). Global, regional, and national burden of stroke and its risk factors, 1990-2019: a systematic analysis for the Global Burden of Disease Study 2019. Lancet Neurol. *20*, 795–820. https://doi.org/10.1016/s1474-4422(21)00252-0.
2. van Rooij, E., Purcell, A.L., and Levin, A.A. (2012). Developing microRNA therapeutics. Circ. Res. *110*, 496–507. https://doi.org/10.1161/circresaha.111.247916.
3. Vyavahare, S., Kumar, S., Smith, K., Mendhe, B., Zhong, R., Cooley, M.A., Baban, B., Isales, C.M., Hamrick, M., Hill, W.D., and Fulzele, S. (2023). Inhibiting MicroRNA-141-3p Improves Musculoskeletal Health in Aged Mice. Aging Dis. *14*, 2303–2316. https://doi.org/10.14336/ad.2023.0310-1.
4. Yadav, S.K., Jauhari, A., Singh, N., Pandey, A., Sarkar, S., Pandey, S., Garg, R.K., Parmar, D., and Yadav, S. (2023). Transcriptomics and Proteomics Approach for the Identification of Altered Blood microRNAs and Plasma Proteins in Parkinson's Disease. Cell. Mol. Neurobiol. *43*, 3527–3553. https://doi.org/10.1007/s10571-023-01362-4.
5. Yadav, S.K., Pandey, A., Sarkar, S., Yadav, S.S., Parmar, D., and Yadav, S. (2022). Identification of Altered Blood MicroRNAs and Plasma Proteins in a Rat Model of Parkinson's Disease. Mol. Neurobiol. *59*, 1781–1798. https://doi.org/10.1007/s12035-021-02636-y.
6. Kehl, T., Backes, C., Kern, F., Fehlmann, T., Ludwig, N., Meese, E., Lenhof, H.P., and Keller, A. (2017). About miRNAs, miRNA seeds, target genes and target pathways. Oncotarget *8*, 107167–107175. https://doi.org/10.18632/oncotarget.22363.
7. Jeyaseelan, K., Lim, K.Y., and Armugam, A. (2008). MicroRNA expression in the blood and brain of rats subjected to transient focal ischemia by middle cerebral artery occlusion. Stroke *39*, 959–966. https://doi.org/10.1161/strokeaha.107.500736.
8. Carlson, A.P., McKay, W., Edwards, J.S., Swaminathan, R., SantaCruz, K.S., Mims, R.L., Yonas, H., and Roitbak, T. (2021). MicroRNA Analysis of Human Stroke Brain Tissue Resected during Decompressive Craniectomy/Stroke-Ectomy Surgery. Genes *12*, 1860. https://doi.org/10.3390/genes12121860.
9. Vasudeva, K., and Munshi, A. (2020). miRNA dysregulation in ischaemic stroke: Focus on diagnosis, prognosis, therapeutic and protective biomarkers. Eur. J. Neurosci. *52*, 3610–3627. https://doi.org/10.1111/ejn.14695.
10. Roitbak, T. (2018). Silencing a Multifunctional microRNA Is Beneficial for Stroke Recovery. Front. Mol. Neurosci. *11*, 58. https://doi.org/10.3389/fnmol.2018.00058.
11. Xu, L.J., Ouyang, Y.B., Xiong, X., Stary, C.M., and Giffard, R.G. (2015). Post-stroke treatment with miR-181 antagomir reduces injury and improves long-term behavioral recovery in mice after focal cerebral ischemia. Exp. Neurol. *264*, 1–7. https://doi.org/10.1016/j.expneurol.2014.11.007.
12. Verma, R., Ritzel, R.M., Harris, N.M., Lee, J., Kim, T., Pandi, G., Vemuganti, R., and McCullough, L.D. (2018). Inhibition of miR-141-3p Ameliorates the Negative Effects of Poststroke Social Isolation in Aged Mice. Stroke *49*, 1701–1707. https://doi.org/10.1161/strokeaha.118.020627.
13. Dhuri, K., Vyas, R.N., Blumenfeld, L., Verma, R., and Bahal, R. (2021). Nanoparticle Delivered Anti-miR-141-3p for Stroke Therapy. Cells *10*, 1011. https://doi.org/10.3390/cells10051011.
14. Rupaimoole, R., Han, H.D., Lopez-Berestein, G., and Sood, A.K. (2011). MicroRNA therapeutics: principles, expectations, and challenges. Chin. J. Cancer *30*, 368–370. https://doi.org/10.5732/cjc.011.10186.
15. Stein, C.A., Subasinghe, C., Shinozuka, K., and Cohen, J.S. (1988). Physicochemical properties of phosphorothioate oligodeoxynucleotides. Nucleic Acids Res. *16*, 3209–3221. https://doi.org/10.1093/nar/16.8.3209.
16. Furdon, P.J., Dominski, Z., and Kole, R. (1989). RNase H cleavage of RNA hybridized to oligonucleotides containing methylphosphonate, phosphorothioate and phosphodiester bonds. Nucleic Acids Res. *17*, 9193–9204. https://doi.org/10.1093/nar/17.22.9193.
17. Jian, H., Xu, G., Yi, Y., Hao, Y., Wang, Y., Xiong, L., Wang, S., Liu, S., Meng, C., Wang, J., et al. (2021). The origin and impeded dissemination of the DNA phosphorothioation system in prokaryotes. Nat. Commun. *12*, 6382. https://doi.org/10.1038/s41467-021-26636-7.
18. Braasch, D.A., and Corey, D.R. (2002). Novel antisense and peptide nucleic acid strategies for controlling gene expression. Biochemistry *41*, 4503–4510. https://doi.org/10.1021/bi0122112.
19. Dias, N., and Stein, C.A. (2002). Antisense oligonucleotides: basic concepts and mechanisms. Mol. Cancer Therapeut. *1*, 347–355.
20. Philippen, L.E., Dirkx, E., Wit, J.B.M., Burggraaf, K., de Windt, L.J., and da Costa Martins, P.A. (2015). Antisense MicroRNA Therapeutics in Cardiovascular Disease: Quo Vadis? Mol. Ther. *23*, 1810–1818. https://doi.org/10.1038/mt.2015.133.
21. Gupta, A., Quijano, E., Liu, Y., Bahal, R., Scanlon, S.E., Song, E., Hsieh, W.C., Braddock, D.E., Ly, D.H., Saltzman, W.M., and Glazer, P.M. (2017). Anti-tumor Activity of miniPEG-γ-Modified PNAs to Inhibit MicroRNA-210 for Cancer Therapy. Mol. Ther. Nucleic Acids *9*, 111–119. https://doi.org/10.1016/j.omtn.2017.09.001.
22. Gupta, A., Bahal, R., Gupta, M., Glazer, P.M., and Saltzman, W.M. (2016). Nanotechnology for delivery of peptide nucleic acids (PNAs). J. Contr. Release *240*, 302–311. https://doi.org/10.1016/j.jconrel.2016.01.005.
23. Dhuri, K., Duran, T., Chaudhuri, B., Slack, F.J., Vikram, A., Glazer, P.M., and Bahal, R. (2023). Head-to-head comparison of *in vitro* and *in vivo* efficacy of pHLIP-conjugated anti-seed gamma peptide nucleic acids. Cell Rep Phys Sci. *4*, 101584. https://doi.org/10.1016/j.xcrp.2023.101584.
24. Malik, S., Slack, F.J., and Bahal, R. (2020). Formulation of PLGA nanoparticles containing short cationic peptide nucleic acids. MethodsX *7*, 101115. https://doi.org/10.1016/j.mex.2020.101115.
25. Wang, Y., Malik, S., Suh, H.W., Xiao, Y., Deng, Y., Fan, R., Huttner, A., Bindra, R.S., Singh, V., Saltzman, W.M., and Bahal, R. (2023). Anti-seed PNAs targeting multiple oncomiRs for brain tumor therapy. Sci. Adv. *9*, eabq7459. https://doi.org/10.1126/sciadv.abq7459.
26. Woodrow, K.A., Cu, Y., Booth, C.J., Saucier-Sawyer, J.K., Wood, M.J., and Saltzman, W.M. (2009). Intravaginal gene silencing using biodegradable polymer nanoparticles densely loaded with small-interfering RNA. Nat. Mater. *8*, 526–533. https://doi.org/10.1038/nmat2444.
27. Oyaghire, S.N., Quijano, E., Piotrowski-Daspit, A.S., Saltzman, W.M., and Glazer, P.M. (2020). Poly(Lactic-co-Glycolic Acid) Nanoparticle Delivery of Peptide Nucleic Acids In Vivo. Methods Mol. Biol. *2105*, 261–281. https://doi.org/10.1007/978-1-0716-0243-0_17.
28. Wahane, A., Malik, S., Shih, K.C., Gaddam, R.R., Chen, C., Liu, Y., Nieh, M.P., Vikram, A., and Bahal, R. (2021). Dual-Modality Poly-l-histidine Nanoparticles to Deliver Peptide Nucleic Acids and Paclitaxel for In Vivo Cancer Therapy. ACS Appl. Mater. Interfaces *13*, 45244–45258. https://doi.org/10.1021/acsami.1c11981.
29. Malik, S., Lim, J., Slack, F.J., Braddock, D.T., and Bahal, R. (2020). Next generation miRNA inhibition using short anti-seed PNAs encapsulated in PLGA nanoparticles. J. Contr. Release *327*, 406–419. https://doi.org/10.1016/j.jconrel.2020.08.026.
30. Peterhans, C., Lally, C.C.M., Ostermaier, M.K., Sommer, M.E., and Standfuss, J. (2016). Functional map of arrestin binding to phosphorylated opsin, with and without agonist. Sci. Rep. *6*, 28686. https://doi.org/10.1038/srep28686.
31. Zahuranec, D.B., and Majersik, J.J. (2012). Percentage of acute stroke patients eligible for endovascular treatment. Neurology *79*, S22–S25. https://doi.org/10.1212/WNL.0b013e31826957cf.
32. Diener, C., Keller, A., and Meese, E. (2022). Emerging concepts of miRNA therapeutics: from cells to clinic. Trends Genet. *38*, 613–626. https://doi.org/10.1016/j.tig.2022.02.006.
33. Khoshnam, S.E., Winlow, W., and Farzaneh, M. (2017). The Interplay of MicroRNAs in the Inflammatory Mechanisms Following Ischemic Stroke. J. Neuropathol. Exp. Neurol. *76*, 548–561. https://doi.org/10.1093/jnen/nlx036.

34. Antony, M., Scranton, V., Srivastava, P., and Verma, R. (2020). Micro RNA 181c-5p: A promising target for post-stroke recovery in socially isolated mice. Neurosci. Lett. *715*, 134610. https://doi.org/10.1016/j.neulet.2019.134610.

35. Malik, S., Pradeep, S.P., Kumar, V., Xiao, Y., Deng, Y., Fan, R., Vasquez, J.C., Singh, V., and Bahal, R. (2024). Antitumor efficacy of a sequence-specific DNA-targeted γPNA-based c-Myc inhibitor. Cell Rep. Med. *5*, 101354. https://doi.org/10.1016/j.xcrm.2023.101354.

36. Dhuri, K., Gaddam, R.R., Vikram, A., Slack, F.J., and Bahal, R. (2021). Therapeutic Potential of Chemically Modified, Synthetic, Triplex Peptide Nucleic Acid-Based Oncomir Inhibitors for Cancer Therapy. Cancer Res. *81*, 5613–5624. https://doi.org/10.1158/0008-5472.Can-21-0736.

37. Bahal, R., Ali McNeer, N., Quijano, E., Liu, Y., Sulkowski, P., Turchick, A., Lu, Y.C., Bhunia, D.C., Manna, A., Greiner, D.L., et al. (2016). In vivo correction of anaemia in β-thalassemic mice by γPNA-mediated gene editing with nanoparticle delivery. Nat. Commun. *7*, 13304. https://doi.org/10.1038/ncomms13304.

38. Demidov, V., Frank-Kamenetskii, M.D., Egholm, M., Buchardt, O., and Nielsen, P.E. (1993). Sequence selective double strand DNA cleavage by peptide nucleic acid (PNA) targeting using nuclease S1. Nucleic Acids Res. *21*, 2103–2107. https://doi.org/10.1093/nar/21.9.2103.

39. Harris, N.M., Ritzel, R., Mancini, N.S., Jiang, Y., Yi, X., Manickam, D.S., Banks, W.A., Kabanov, A.V., McCullough, L.D., and Verma, R. (2016). Nano-particle delivery of brain derived neurotrophic factor after focal cerebral ischemia reduces tissue injury and enhances behavioral recovery. Pharmacol. Biochem. Behav. *150–151*, 48–56. https://doi.org/10.1016/j.pbb.2016.09.003.

40. Daneman, R., and Prat, A. (2015). The blood-brain barrier. Cold Spring Harbor Perspect. Biol. *7*, a020412. https://doi.org/10.1101/cshperspect.a020412.

41. Masserini, M. (2013). Nanoparticles for brain drug delivery. ISRN Biochem. *2013*, 238428. https://doi.org/10.1155/2013/238428.

42. Chiu, H.I., Samad, N.A., Fang, L., and Lim, V. (2021). Cytotoxicity of targeted PLGA nanoparticles: a systematic review. RSC Adv. *11*, 9433–9449. https://doi.org/10.1039/d1ra00074h.

43. Ayyaz, A., Attisano, L., and Wrana, J.L. (2017). Recent advances in understanding contextual TGFβ signaling. F1000Res. *6*, 749. https://doi.org/10.12688/f1000research.11295.1.

44. Travis, M.A., and Sheppard, D. (2014). TGF-β activation and function in immunity. Annu. Rev. Immunol. *32*, 51–82. https://doi.org/10.1146/annurev-immunol-032713-120257.

45. Schmierer, B., and Hill, C.S. (2007). TGFbeta-SMAD signal transduction: molecular specificity and functional flexibility. Nat. Rev. Mol. Cell Biol. *8*, 970–982. https://doi.org/10.1038/nrm2297.

46. Zhang, L., Wei, W., Ai, X., Kilic, E., Hermann, D.M., Venkataramani, V., Bähr, M., and Doeppner, T.R. (2021). Extracellular vesicles from hypoxia-preconditioned microglia promote angiogenesis and repress apoptosis in stroke mice via the TGF-β/Smad2/3 pathway. Cell Death Dis. *12*, 1068. https://doi.org/10.1038/s41419-021-04363-7.

47. Zhang, S.Z., Wang, Q.Q., Yang, Q.Q., Gu, H.Y., Yin, Y.Q., Li, Y.D., Hou, J.C., Chen, R., Sun, Q.Q., Sun, Y.F., et al. (2019). NG2 glia regulate brain innate immunity via TGF-β2/TGFBR2 axis. BMC Med. *17*, 204. https://doi.org/10.1186/s12916-019-1439-x.

48. Cavaillon, J.M. (2001). Pro- versus anti-inflammatory cytokines: myth or reality. Cell. Mol. Biol. *47*, 695–702.

49. Simats, A., and Liesz, A. (2022). Systemic inflammation after stroke: implications for post-stroke comorbidities. EMBO Mol. Med. *14*, e16269. https://doi.org/10.15252/emmm.202216269.

50. Hou, D., Wang, C., Ye, X., Zhong, P., and Wu, D. (2021). Persistent inflammation worsens short-term outcomes in massive stroke patients. BMC Neurol. *21*, 62. https://doi.org/10.1186/s12883-021-02097-9.

51. Milosevich, E., Demeyere, N., and Pendlebury, S.T. (2024). Infection, Inflammation, and Poststroke Cognitive Impairment. J. Am. Heart Assoc. *13*, e9130. https://doi.org/10.1161/jaha.123.033015.

52. Jeon, Y.K., and Ha, C.H. (2015). Expression of brain-derived neurotrophic factor, IGF-1 and cortisol elicited by regular aerobic exercise in adolescents. J. Phys. Ther. Sci. *27*, 737–741. https://doi.org/10.1589/jpts.27.737.

53. McCusker, R.H., McCrea, K., Zunich, S., Dantzer, R., Broussard, S.R., Johnson, R.W., and Kelley, K.W. (2006). Insulin-like growth factor-I enhances the biological activity of brain-derived neurotrophic factor on cerebrocortical neurons. J. Neuroimmunol. *179*, 186–190. https://doi.org/10.1016/j.jneuroim.2006.06.014.

54. Verma, R., Friedler, B.D., Harris, N.M., and McCullough, L.D. (2014). Pair housing reverses post-stroke depressive behavior in mice. Behav. Brain Res. *269*, 155–163. https://doi.org/10.1016/j.bbr.2014.04.044.

55. Srivastava, P., Cronin, C.G., Scranton, V.L., Jacobson, K.A., Liang, B.T., and Verma, R. (2020). Neuroprotective and neuro-rehabilitative effects of acute purinergic receptor P2X4 (P2X4R) blockade after ischemic stroke. Exp. Neurol. *329*, 113308. https://doi.org/10.1016/j.expneurol.2020.113308.

56. Verma, R., Cronin, C.G., Hudobenko, J., Venna, V.R., McCullough, L.D., and Liang, B.T. (2017). Deletion of the P2X4 receptor is neuroprotective acutely, but induces a depressive phenotype during recovery from ischemic stroke. Brain Behav. Immun. *66*, 302–312.

57. Moy, S.S., Nikolova, V.D., Riddick, N.V., Baker, L.K., and Koller, B.H. (2012). Preweaning sensorimotor deficits and adolescent hypersociability in Grin1 knockdown mice. Dev. Neurosci. *34*, 159–173. https://doi.org/10.1159/000337984.

58. Truong, D.T., Venna, V.R., McCullough, L.D., and Fitch, R.H. (2012). Deficits in auditory, cognitive, and motor processing following reversible middle cerebral artery occlusion in mice. Exp. Neurol. *238*, 114–121. https://doi.org/10.1016/j.expneurol.2012.08.011.

59. Agarwal, V., Bell, G.W., Nam, J.W., and Bartel, D.P. (2015). Predicting effective microRNA target sites in mammalian mRNAs. Elife *4*, e05005. https://doi.org/10.7554/eLife.05005.

60. Huang, H.Y., Lin, Y.C.D., Cui, S., Huang, Y., Tang, Y., Xu, J., Bao, J., Li, Y., Wen, J., Zuo, H., et al. (2022). miRTarBase update 2022: an informative resource for experimentally validated miRNA-target interactions. Nucleic Acids Res. *50*, D222–D230. https://doi.org/10.1093/nar/gkab1079.

61. Verma, R., Harris, N.M., Friedler, B.D., Crapser, J., Patel, A.R., Venna, V., and McCullough, L.D. (2016). Reversal of the Detrimental Effects of Post-Stroke Social Isolation by Pair-Housing is Mediated by Activation of BDNF-MAPK/ERK in Aged Mice. Sci. Rep. *6*, 25176. https://doi.org/10.1038/srep25176.